

International Journal of Modern Physics E
 © World Scientific Publishing Company

Microscopic formulation of the interacting boson model for reflection asymmetric nuclei

Kosuke Nomura

*Department of Physics, University of Zagreb
 Zagreb, HR-10000, Croatia
 knomura@phy.hr*

Received Day Month Year

Revised Day Month Year

Reflection asymmetric, octupole shapes in nuclei are a prominent aspect of nuclear structure, and have been recurrently studied over the decades. Recent experiments using radioactive-ion beams have provided evidence for stable octupole shapes. A variety of nuclear models have been employed for the related theoretical analyses. We review recent studies on the nuclear octupole shapes and collective excitations within the interacting boson model. A special focus is placed on the microscopic formulation of this model by using the mean-field method that is based on the framework of nuclear density functional theory. As an illustrative example, a stable octupole deformation, and a shape phase transition as a function of nucleon number that involves both quadrupole and octupole degrees of freedom are shown to occur in light actinides. Systematic spectroscopic studies indicate enhancement of the octupole collectivity in a wide mass region. Couplings between the octupole and additional degrees of freedom are incorporated in a microscopic manner in the boson system, and shown to play a crucial role in the description of the related intriguing nuclear structure phenomena such as the shape coexistence.

Keywords: Octupole deformation; interacting boson model; mean-field model; density functional theory; shape phase transition; shape coexistence.

PACS numbers: 21.10.Re, 21.60.Ev, 21.60.Fw, 21.60.Jz

1. Introduction

Reflection asymmetric, octupole deformation of the atomic nuclei presents a theme of great interest in nuclear structure physics.^{1,2} The octupole deformation is expected to emerge in those mass regions in the chart of nuclides in which a coupling occurs between the single-particle orbitals that differ by $\Delta\ell = \Delta j = 3\hbar$ (ℓ and j are quantum numbers of single-particle state) and are opposite in parity. Empirical signatures of the octupole deformation are low-energy negative-parity states forming an alternating parity band with the positive-parity yrast states, and enhanced electric dipole and octupole transitions within the band.

The existence of low-lying negative-parity states that are associated with the reflection asymmetric deformation was recognized in the 1950's. Since then the topic

has been recurrently pursued. Recent experiments using radioactive-ion-beams have identified evidence for stable octupole shapes, e.g., in light actinides^{3–5} and lanthanides.^{6,7} Besides that, theoretical studies that are to support and predict the occurrence of nuclear octupole states have been extensively conducted using a variety of nuclear structure models. An extensive list of the relevant experimental and theoretical studies is given in the review articles, e.g., Refs. 1, 2. In addition, the presence of static octupole correlations in the nucleus enhances an atomic electric dipole moment (EDM). The observation of a non-zero EDM would imply the violation of the CP symmetry, hence is important for exploring new physics beyond the standard model of elementary particles.⁸

In this paper, we review recent theoretical investigations on the reflection asymmetric nuclear shapes and related collective states within the interacting boson model (IBM).⁹ A special focus is placed on the microscopic formulation of this model in terms of the nuclear mean-field method. Within this theoretical scheme a stable octupole shape emerges in a characteristic set of nuclei in which octupole deformation is empirically suggested to occur. A transition between the quadrupole and octupole states as functions of the nucleon number is discussed in the context of the quantum phase transition in nuclear shapes.¹⁰ Coupling between single-particle and collective octupole degrees of freedom is shown to play an important role in determining the low-lying band structure of the odd-mass nuclei. Furthermore the octupole correlations are shown to be relevant for understanding the nature of the low-energy excited 0^+ states, which are often considered as a signature of shape coexistence.^{11,12}

2. Interacting boson model for reflection asymmetric nuclei

The IBM, proposed by Arima and Iachello,^{9,13} has been remarkably successful in reproducing low-energy quadrupole collective states in a large number of medium-heavy and heavy nuclei. Its basic assumption is that the multi-fermion dynamics of the nuclear surface deformation is simulated in terms of the monopole, s , and quadrupole, d , bosons, which represent, from a microscopic point of view,^{9,14,15} collective S and D pairs of valence nucleons corresponding to spin and parity 0^+ and 2^+ , respectively. This corresponds to a drastic truncation of the full shell model configuration space which becomes prohibitively large for heavy and open-shell nuclei. The model is also intimately related to the group theory. A prominent feature is the emergence of the dynamical symmetry, i.e., if the Hamiltonian is written as a specific combination of Casimir operators then the Hamiltonian is associated with a certain intrinsic structure and is exactly solvable. The sd -IBM, for instance, constitutes the bosonic algebra $U(6)$, and from it appear three subalgebras $U(5)$, $SU(3)$, and $O(6)$, which correspond to vibrational, rotational, and γ -unstable limits of the quadrupole mode, respectively.

To study negative-parity states, the IBM was extended^{16–19} so that the boson model space should contain, in addition to the positive-parity s and d bosons, the

negative-parity bosons such as the dipole, p , and octupole, f , bosons representing the spin and parity 1^- and 3^- nucleon pairs, respectively. The *spdf*- and *sdf*-boson models have been employed in phenomenological studies on the quadrupole-octupole coupled collective excitations in realistic cases in actinides,²⁰ rare-earth²¹ and lanthanides.²² From a group theoretical point of view, the *sdf*- and *spdf*-boson models constitute, respectively, the boson algebras $U(13)$ and $U(16)$. The group structures including the dynamical symmetries of the quadrupole and octupole states have been analyzed in this respect.^{17, 18, 23, 24}

Besides numerous successes in reproducing observed collective spectra, the IBM should have its microscopic basis on nucleonic degrees of freedom, and attempts have been made to establish a link between the IBM and more microscopic nuclear structure models. A standard method, referred to as the Otsuka-Arima-Iachello (OAI) mapping,^{14, 15} is such that a seniority-based shell-model state given in terms of the S , D , \dots nucleon pairs is mapped onto the equivalent s , d , \dots boson state. The number of bosons is set equal to that of the valence nucleons. The OAI method has been shown to be valid in limited realistic cases of moderately deformed nuclei, i.e., nearly spherical and γ -unstable ones.²⁵

More recently, making use of the fact that the potential energy surface of a given nuclear mean-field model can be simulated by that of the boson system, the IBM Hamiltonian has been shown²⁶ to be derived in the general situations of quadrupole collective mode, covering the nearly spherical vibrational $[U(5)]$,^{26, 27} strongly deformed rotational $[SU(3)]$,²⁸ γ -unstable $[O(6)]$,^{26, 27} and triaxially deformed states.²⁹ The method was extended further to address various problems in nuclear structure, including the shape coexistence,³⁰ octupole deformation and collectivity,^{31–33} description of odd-mass nuclei,³⁴ and nuclear β decays.^{35, 36} In what follows, we outline the above-mentioned method and discuss its applications to those nuclear properties in which octupole correlations are expected to be relevant.

3. Mean-field derivation of the interacting boson model

3.1. Mean-field calculations

Among contemporary theoretical approaches, the nuclear density functional theory (DFT)^{37–41} allows for a global and accurate prediction of bulk nuclear matter and intrinsic properties of finite nuclei, including the mass, radii, deformations, etc., and collective excitations over the entire region of the nuclear chart. Its basic implementation is in the self-consistent mean-field (SCMF) calculations, in which an energy density functional (EDF) is constructed as a functional of one-body density matrices that correspond to a single product state. Both nonrelativistic^{37, 40} and relativistic^{38, 39} EDFs have been successfully applied to numerous studies on nuclear structure phenomena.

The starting point is a set of constrained SCMF calculations⁴² for each nucleus to obtain the potential energy surface, that is, the total mean-field energy as a function of the relevant shape degrees of freedom. Here the constraints are on the

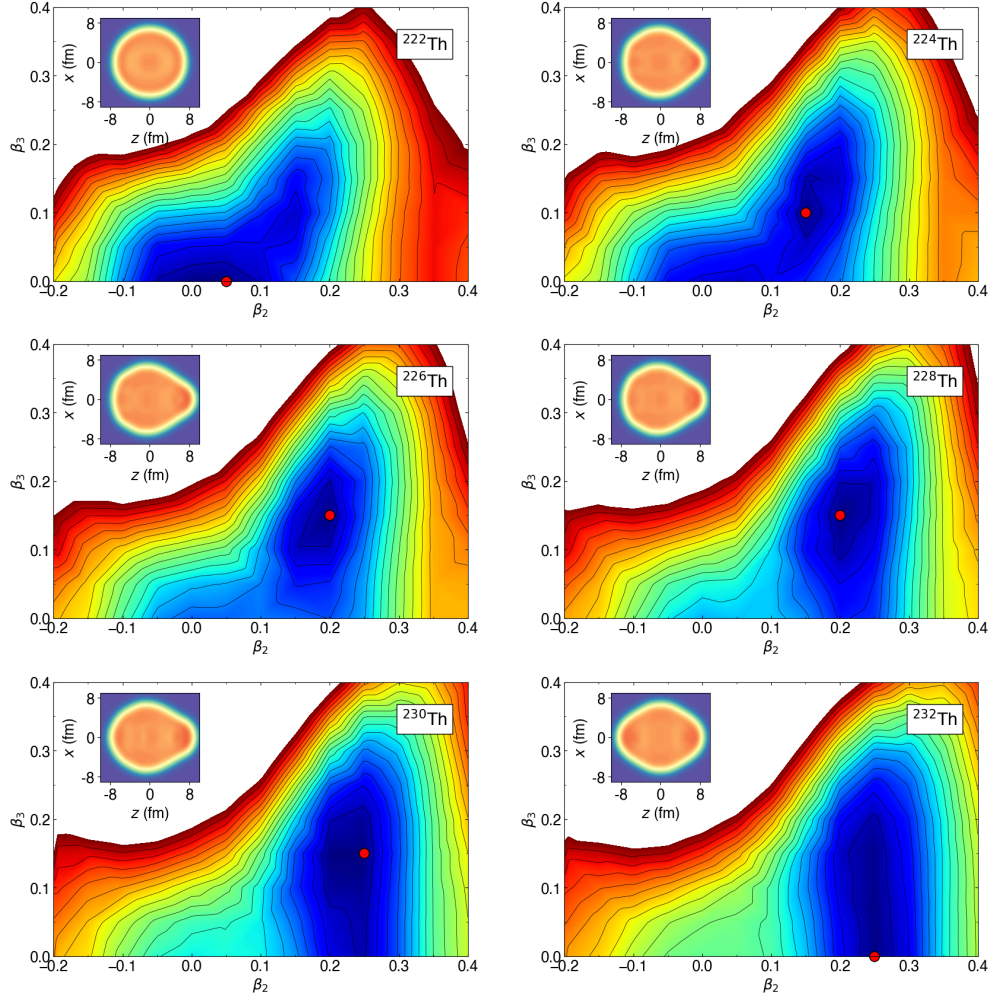
4 *Kosuke Nomura*

Fig. 1. Potential energy surfaces for $^{222-232}\text{Th}$ in terms of the axially-symmetric quadrupole β_2 and octupole β_3 deformations, calculated within the relativistic Hartree-Bogoliubov method using the functional DD-PC1 and separable pairing force. The energy surface is plotted up to 10 MeV from the global minimum, indicated by the solid red circle. The energy difference between the neighboring contour lines is 0.5 MeV. The calculated intrinsic nucleon density in the x - z plane is also shown for each nucleus.

axially symmetric intrinsic quadrupole Q_{20} and octupole Q_{30} moments, which are related to the deformation variables β_2 and β_3 , respectively.

As an illustrative example, Fig. 1 shows the mean-field potential energy surfaces for the axially symmetric even-even nuclei $^{222-232}\text{Th}$. The SCMF calculations are performed within the relativistic Hartree-Bogoliubov (RHB) method^{38,39} based on the density-dependent point-coupling (DD-PC1)⁴³ interaction and the separable

pairing force of finite range.⁴⁴ Variation of the topology of energy surface as a function of nucleon number gives a qualitative interpretation of nuclear shape evolution. The global (equilibrium) minimum occurs at nearly spherical mean-field configuration $(\beta_2, \beta_3) \approx (0.05, 0.0)$ for ^{222}Th . In the neighboring isotope ^{224}Th a non-zero octupole minimum with $\beta_3 \approx 0.1$ is seen. The octupole deformation becomes most pronounced for ^{226}Th . Note the occurrence of the stable octupole minimum is inferred by the behaviors of the single-particle levels near the Fermi energies; At the deformations that correspond to the octupole global minimum, level densities of the single proton and neutron orbits were indeed shown to be lower near the Fermi energies.⁴⁵ For heavier nuclei $^{228,230}\text{Th}$, the energy surface becomes softer along the β_3 direction. For ^{232}Th , the octupole minimum disappears, but the potential is substantially soft in the β_3 deformation.

Figure 1 also shows total intrinsic nucleon density in the x - z plane for each nucleus, computed within the RHB method with the constraints on those β_2 and β_3 deformations corresponding to the global minimum. One finds the intrinsic nucleon densities resembling a completely spherically symmetric shape for ^{222}Th , a reflection asymmetric shape for $^{224-230}\text{Th}$, and a reflection symmetric shape for ^{232}Th .

3.2. Mapping onto the boson system

Let us turn to the boson system. We employ the simplest version of the *sdf*-boson model, where no distinction is made between proton and neutron bosons. A form of the *sdf*-IBM Hamiltonian appropriate for realistic calculations^{31,32} reads

$$\hat{H}_B = \epsilon_d \hat{n}_d + \epsilon_f \hat{n}_f + \kappa_2 \hat{Q} \cdot \hat{Q} + \kappa'_2 \hat{L}_d \cdot \hat{L}_d + \kappa_3 : \hat{V}_3^\dagger \cdot \hat{V}_3 : . \quad (1)$$

$\hat{n}_d = d^\dagger \cdot \tilde{d}$ and $\hat{n}_f = f^\dagger \cdot \tilde{f}$ are number operators for d and f bosons, with ϵ_d and ϵ_f being single- d and $-f$ boson energies relative to the s boson one, respectively. Note that $\tilde{d}_\mu = (-1)^{-\mu} d_{-\mu}$, $\tilde{f}_\mu = (-1)^{3-\mu} f_{-\mu}$, and the dot (\cdot) means scalar product. The third term in Eq. (1) is the quadrupole-quadrupole interaction with the strength parameter κ_2 , and $\hat{Q} = s^\dagger \tilde{d} + d^\dagger s + \chi_d [d^\dagger \times \tilde{d}]^{(2)} + \chi_f [f^\dagger \times \tilde{f}]^{(2)}$ is the quadrupole operator. χ_d and χ_f are dimensionless parameters. The fourth term, with the strength κ'_2 , is specifically required for strongly axially deformed nuclei,²⁸ and \hat{L}_d is the angular momentum operator for d bosons $\hat{L}_d = \sqrt{10} [d^\dagger \times \tilde{d}]^{(1)}$. The last term, expressed in the normal-ordered form, represents the octupole-octupole interaction with the strength parameter κ_3 , and the operator $\hat{V}_3^\dagger = s^\dagger \tilde{f} + \chi_3 [d^\dagger \times \tilde{f}]^{(3)}$, with χ_3 being another dimensionless parameter. For details, see Ref. 32.

A given boson model Hamiltonian can be related to a certain geometrical structure by using the boson coherent state.⁴⁶⁻⁴⁸ For the *sdf*-IBM, if axial symmetry is assumed the coherent state $|\phi\rangle$ is expressed as

$$|\phi\rangle = (n!)^{-1/2} (\lambda^\dagger)^n |0\rangle, \quad \lambda^\dagger = (1 + \tilde{\beta}_2^2 + \tilde{\beta}_3^2)^{-1/2} (s^\dagger + \tilde{\beta}_2 d_0^\dagger + \tilde{\beta}_3 f_0^\dagger). \quad (2)$$

Here, n denotes the number of bosons, and $|0\rangle$ is the boson vacuum, i.e., the inert core. The amplitudes $\tilde{\beta}_2$ and $\tilde{\beta}_3$ are considered as the boson analogs of β_2 and β_3

6 *Kosuke Nomura*

deformations in the geometrical model. The energy surface of the boson system, denoted by $E_{\text{IBM}}(\tilde{\beta}_2, \tilde{\beta}_3)$, is obtained by taking an expectation value $\langle \phi | \hat{H}_{\text{B}} | \phi \rangle$, which also depends on the parameters of the Hamiltonian \hat{H}_{B} (1). To a good approximation, the bosonic deformation variables $(\tilde{\beta}_2, \tilde{\beta}_3)$ are connected to the fermionic counterparts (β_2, β_3) through the relations^{26, 32, 46}

$$\tilde{\beta}_2 = c_2 \beta_2, \quad \tilde{\beta}_3 = c_3 \beta_3, \quad (3)$$

with c_2 and c_3 being constants of proportionality. Typical values for these constants are ~ 5 . The fact that the bosonic deformations are larger than the fermionic ones reflects that the IBM is built on the limited configuration (valence) space while the SCMF model considers all nucleons in the nucleus.

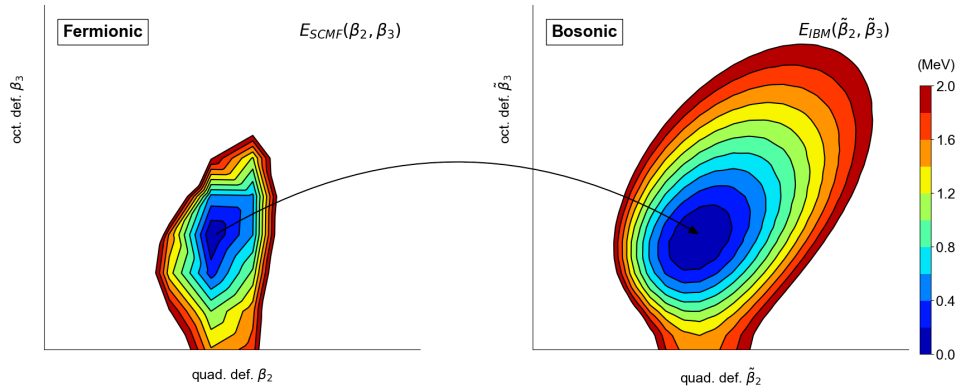


Fig. 2. A schematic illustration of the mapping of the fermionic potential energy surface $E_{\text{SCMF}}(\beta_2, \beta_3)$ onto the bosonic counterpart $E_{\text{IBM}}(\tilde{\beta}_2, \tilde{\beta}_3)$.

Together with the relations in (3), the SCMF and IBM potential energy surfaces are equated to each other:

$$E_{\text{SCMF}}(\beta_2, \beta_3) \sim E_{\text{IBM}}(\tilde{\beta}_2, \tilde{\beta}_3). \quad (4)$$

This procedure represents a mapping of the fermionic energy surface onto the bosonic one, as schematically illustrated in Fig. 2. The parameters of the Hamiltonian \hat{H}_{B} , and the proportionality constants c_2 and c_3 for the deformation variables are determined by the mapping procedure. In other words, the IBM parameters are derived so that the bosonic energy surface becomes similar to the fermionic one as much as possible. Note that the relation (4) is an approximate equality that should be satisfied within a limited range of the (β_2, β_3) space, that is, in the vicinity of the global minimum. This is based on the fact that the low-energy quadrupole and octupole collective states are predominantly accounted for by the SCMF solutions near the global minimum.^{26, 27, 45, 49}

In addition, since the parameter κ'_2 for the rotational term $\hat{L}_d \cdot \hat{L}_d$ [see Eq. (1)] cannot be uniquely determined from the comparison of the potential energy surfaces, it is derived separately,²⁸ from the comparison of the intrinsic moment of inertia in the boson system to the fermionic one computed in the cranking approximation.

Having determined the parameters for \hat{H}_B by the mapping procedure, the resultant IBM Hamiltonian is numerically diagonalized, resulting in the energies and wave functions of the excited states of both parities. It should be noted that no phenomenological adjustment is made in this procedure, that is, the *sdf*-IBM Hamiltonian is determined only by using inputs provided by the microscopic calculations within the EDF framework, which is also not specifically adjusted to the observed octupole states.

At this point, it is worth mentioning that the octupole shapes and collective excitations have also been extensively studied by a number of beyond-mean-field approaches within the EDF framework, including the symmetry projected generator coordinate method (see, e.g., Refs. 40, 50, and an extensive list of references are therein) and the quadrupole-octupole collective model.^{49,51,52}

3.3. Octupole shape phase transitions in Th isotopes

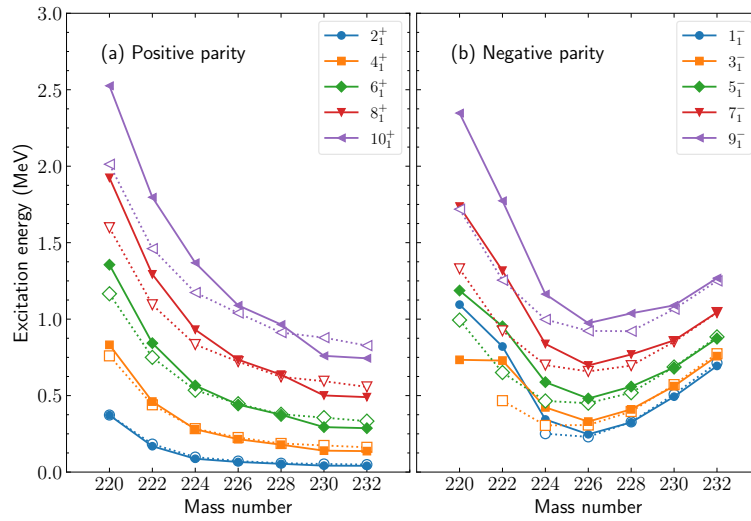


Fig. 3. Evolution of the excitation energies for the (a) positive- and (b) negative-parity yrast states for $^{220-232}\text{Th}$. Solid (open) symbols represent the calculated (experimental) values, and are connected by solid (broken) lines.

Figure 3 shows the calculated energy spectra for the even-spin positive-parity and odd-spin negative-parity yrast states for $^{220-232}\text{Th}$. Agreement between the

calculated and experimental⁵³ energy spectra is good. As one sees in Fig. 3(a), the overall decrease in energy of the positive-parity levels indicates a transition from vibrational to rotational nuclear structures. The negative-parity levels, on the other hand, exhibit a characteristic parabolic behavior with the minimum energy at ^{226}Th . [see Fig. 3(b)]. Around ^{226}Th , bands with both parities are close to each other, and appear to form an approximate alternating parity band as expected for a stable octupole state. For $A > 226$, the negative-parity levels keep rising with mass number, while the positive-parity ones gradually decrease. Toward the nucleus ^{232}Th , the positive- and negative-parity bands are almost decoupled from each other, and appear to form separate $\Delta I = 2$ rotational bands.

To identify the occurrence of the alternating-parity band structure in the Th isotopes, it is convenient to study the signature splitting:

$$S(I) = \frac{[E(I+1) - E(I)] - [E(I) - E(I-1)]}{E(2_1^+)}. \quad (5)$$

$E(I)$ stands for the excitation energies of the $I = 1_1^-, 2_1^+, 3_1^-, 4_1^+, \dots$ states. The quantity $S(I)$ is sensitive to the splitting between the positive- and negative-parity rotational bands. For an ideal alternating parity band, the positive- and negative-parity bands should appear with an equal energy splitting, hence $S(I) \approx 0$. Non-zero $S(I)$ value would indicate a deviation from the pure alternating parity band. This situation is illustrated in Fig. 4. For $^{220-226}\text{Th}$, the $S(I)$ value is nearly equal to zero. For $^{228-232}\text{Th}$, in turn, the odd-even spin staggering occurs, and the deviation from the limit $S(I) = 0$ becomes even larger with mass number.

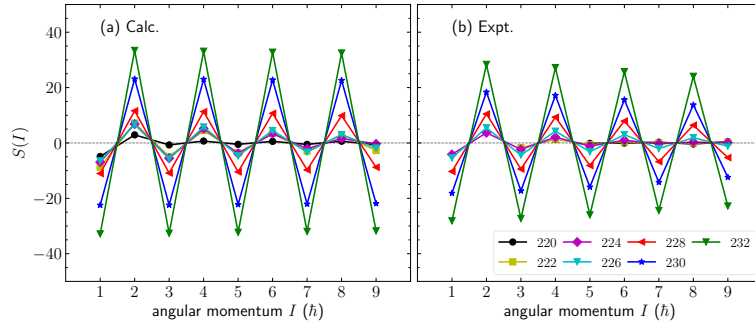


Fig. 4. Calculated (a) and experimental⁵³ (b) signature splittings $S(I)$ between the even- I positive-parity and odd- I negative-parity bands for $^{220-230}\text{Th}$ as functions of the angular momentum.

The systematic behavior of the calculated energy spectra for the yrast bands with both parities, point to the occurrence of a type of quantum phase transition¹⁰ along the chain of Th isotopes, that is, the structural evolution from nearly spherical to stable octupole shapes toward ^{226}Th , and to an octupole vibrational state around $^{230,232}\text{Th}$ associated with the octupole-soft potential. The behavior of the calculated

spectroscopic properties reflects, to a large extent, the variation of the topology of the SCMF energy surface in the β_2 - β_3 plane, as was shown in Fig. 1. In addition, the Th isotopes appears to be an ideal case that exhibits a stable octupole deformation, as well as a shape phase transition that involves quadrupole and octupole modes.

4. Global study

The octupolarity is suggested to be enhanced in several different mass regions, corresponding to the neutron and proton numbers $(N, Z) \approx (134, 88)$, $(88, 56)$ $(56, 56)$, $(56, 34)$, $(34, 34)$, \dots , at which the $\Delta\ell = \Delta j = 3\hbar$ coupling between the single-particle orbitals can occur.

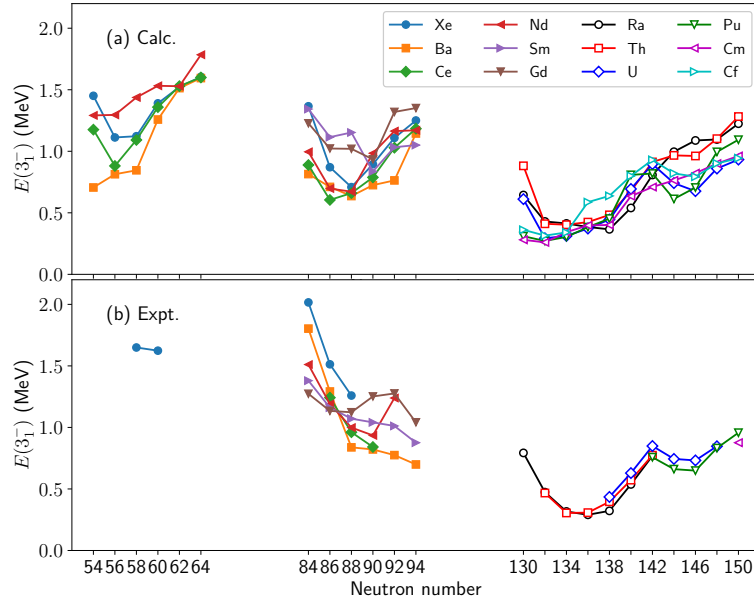


Fig. 5. Evolution of (a) calculated and (b) experimental 3_1^- excitation energies as functions of the neutron number along those isotopic chains characteristic of the octupole deformation.

Figure 5 shows the calculated 3_1^- excitation energies for the nuclei in those characteristic mass regions in which octupole deformation is expected to occur. The plot has been made as a compilation of the results^{33, 50, 54–56} obtained from the *sdf*-IBM that is based on the Hartree-Fock-Bogoliubov (HFB) calculations using the Gogny-D1M⁵⁷ EDF.⁵⁸ In general, the predicted 3_1^- energy shows a parabolic behavior that is centered around $N = 56$, 88 , and 134 . This tendency is consistent with what is suggested experimentally, apart from the Ba and Sm isotopes. In many of the nuclei in the light actinides close to $N = 134$, the 3^- state appears at substantially low excitation energy $E_x < 0.5$ MeV. The corresponding Gogny-

HFB SCMF calculations indeed give an octupole-deformed ($\beta_3 \neq 0$) equilibrium minimum for these actinide nuclei.^{50,54} One notices in Fig. 5 another parabolic variation of the 3^- level around $N = 146$. This local behavior implies the effect of dynamical octupole correlations that could be important even away from the neutron number $N = 134$. The 3^- energy is calculated to be rather high for the neutron-deficient Ba region with $54 \leq N \leq 64$. In this region, therefore, the octupole correlations appear to be relatively weak. It is also noted that for the nuclei with $N \approx Z$, some additional correlations such as the neutron-proton pairs may play a role, which are, however, not taken into account in the present calculations.

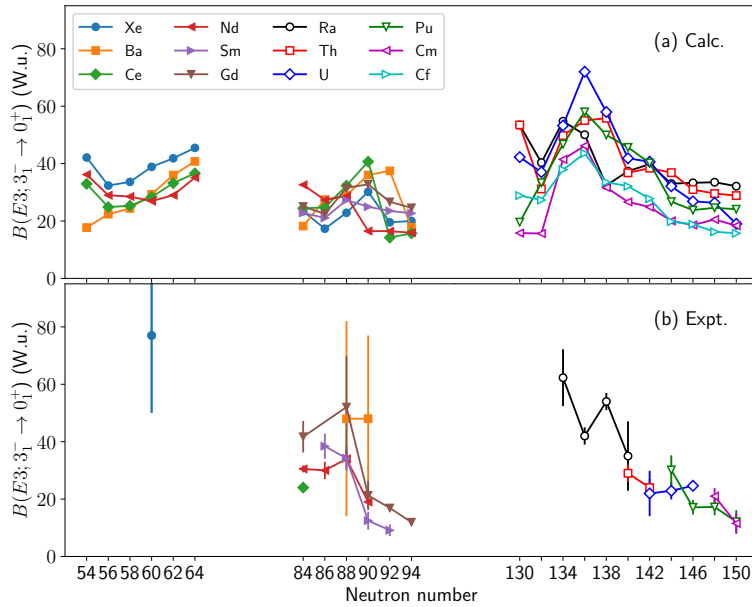


Fig. 6. (a) Calculated and (b) experimental^{6,7,53,59,60} $B(E3; 3_1^- \rightarrow 0_1^+)$ transition probabilities for the same nuclei as those considered in Fig. 5.

The electric octupole ($E3$) transition probability $B(E3; 3_1^- \rightarrow 0_1^+)$ is another indicator of the enhanced octupole collectivity. Figure 6 shows the $B(E3; 3_1^- \rightarrow 0_1^+)$ values for the same nuclei as those shown in Fig. 5, computed by the *sdf*-IBM with the microscopic input from the same Gogny-HFB calculations.^{33,50,54-56} For the $E3$ transition operator, the standard boson $E3$ effective charges that are often used in realistic *sdf*-IBM calculations are chosen.^{33,50,54-56} The calculated $B(E3; 3_1^- \rightarrow 0_1^+)$ rate exhibits an inverse parabolic behavior exhibiting a maximum value around $N = 88$ and 134 . This behavior corroborates the one obtained for the 3^- energy level (see Fig. 5), and is consistent with the data.

5. Coupling with additional degrees of freedom

5.1. Particle-boson coupling in odd-mass systems

Octupole correlations are expected to be relevant to the low-lying states of odd-mass nuclei, as well as to the even-even ones. To treat odd-mass nuclear systems, coupling between a single-particle (or unpaired nucleon) degree of freedom and collective even-even boson space is considered within the interacting boson-fermion model (IBFM).^{61,62} The IBFM Hamiltonian consists of the IBM Hamiltonian \hat{H}_B , single-nucleon Hamiltonian \hat{H}_F , and a term \hat{V}_{BF} representing the boson-fermion coupling:

$$\hat{H}_{\text{IBFM}} = \hat{H}_B + \hat{H}_F + \hat{V}_{BF}. \quad (6)$$

Here, \hat{H}_B was defined in Eq. (1), and $\hat{H}_F = \sum_j \epsilon_j a_j^\dagger \cdot \tilde{a}_j$, with $a_j^{(\dagger)}$ and ϵ_j being the annihilation (creation) operator of a nucleon in the orbital j and the single-particle energy, respectively. The interaction \hat{V}_{BF} consists of the monopole, dynamical quadrupole and octupole, and exchange terms.⁶³ By using the generalized seniority scheme,^{63,64} coefficients of the boson-fermion interaction terms are shown to be given as functions of particle occupation numbers (v_j^2).

As an illustrative example, let us consider the nucleus ^{145}Ba , a system of a single neutron coupled to the even-even nucleus ^{144}Ba . Experimentally, a static octupole deformation has been identified in ^{144}Ba ,⁶ while the octupole correlations have been suggested to be present in the odd-mass neighbor ^{145}Ba .⁶⁵ For the single-particle space of the odd neutron we include the entire $N = 82$ -126 neutron major oscillator shell consisting of the $3p_{1/2}$, $3p_{3/2}$, $2f_{5/2}$, $2f_{7/2}$, $1h_{9/2}$, and $1i_{13/2}$ orbits.

The procedure to fix the IBFM Hamiltonian in Eq. (6) goes as follows.^{34,63} First, the *sd*f-IBM Hamiltonian \hat{H}_B is determined by the β_2 - β_3 energy-surface mapping as described in Sec. 3.2. Second, the spherical single-particle energies ϵ_j and occupation probabilities v_j^2 , which enter \hat{H}_F and \hat{V}_{BF} , respectively, are provided by the SCMF calculation constrained to zero quadrupole and octupole deformations. Finally, only the strength parameters for the boson-fermion interactions are treated as free parameters, and are fitted to reproduce the empirical low-energy spectra of the odd-mass nucleus.

Figure 7 shows SCMF axially-symmetric β_2 - β_3 energy surface for the even-even core ^{144}Ba , obtained from the RHB method that employs the functional DD-PC1 and the separable pairing force. One clearly sees an octupole deformed minimum at $(\beta_2, \beta_3) \approx (0.22, 0.14)$, suggesting a pronounced octupole collectivity. The intrinsic nucleon density projected on the x - z plane, also shown in Fig. 7, indeed resembles a reflection-asymmetric nuclear shape.

In Fig. 8, low-energy excitation spectra for the positive- and negative-parity yrast states of ^{144}Ba resulting from the *sd*f-IBM are compared with the experimental data.⁶ For states belonging to the negative-parity yrast band, the matrix element of the f -boson number operator is calculated to be $\langle \hat{n}_f \rangle \approx 1$, that is, the band is mainly constructed by one- f boson ($n_f = 1$) components coupled with the

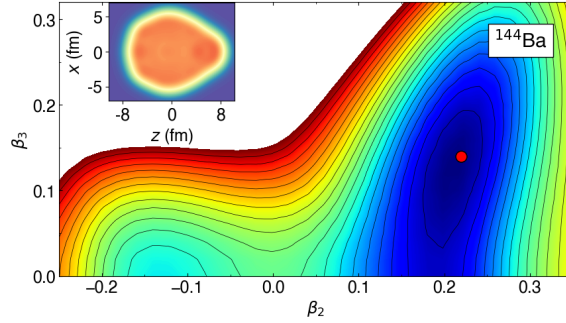
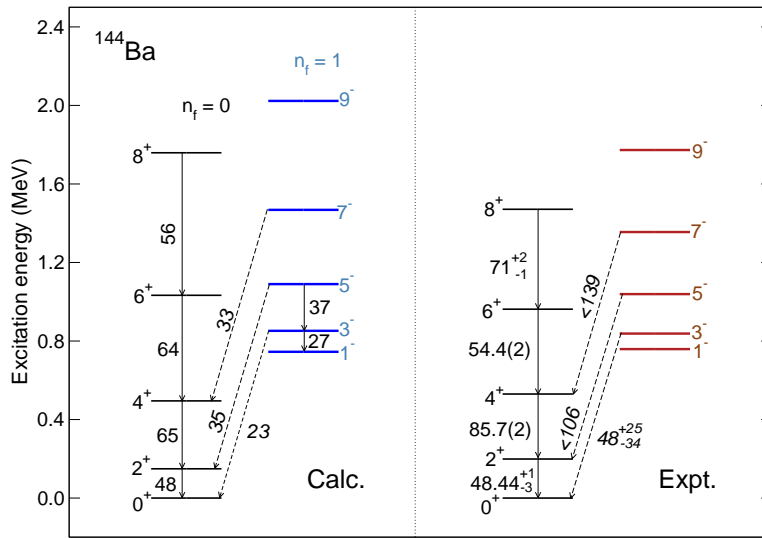
Fig. 7. Same as Fig. 1, but for ^{144}Ba .

Fig. 8. Calculated and experimental⁶ low-energy excitation spectra for positive- and negative-parity yrast states of ^{144}Ba . Numbers along solid and dotted lines are $B(E2)$ and $B(E3)$ values in W.u., respectively. The calculated positive- and negative-parity states are made of zero ($n_f = 0$) and one ($n_f = 1$) f boson configurations, respectively. The DD-PC1 EDF is employed for the microscopic input to the sdf -IBM.

sd boson space. The positive-parity band is, however, solely made of the sd bosons, as $\langle n_f \rangle \approx 0$. The calculated $B(E3; 3_1^- \rightarrow 0_1^+)$ transition probability of 23 W.u. is comparable to the measured value, 48_{-34}^{+25} W.u.

The low-energy excitation spectra for the neighboring odd-mass nucleus ^{145}Ba computed by the sdf -IBFM are given in Fig. 9. The sdf -IBFM wave functions for the lowest two $5/2^-$ and $7/2^-$ negative-parity band are mainly composed of the configuration of the odd neutron in the $1h_{9/2}$ orbit coupled to the sd boson space, with the matrix element $\langle n_f \rangle \approx 0$. The lowest positive-parity band with the

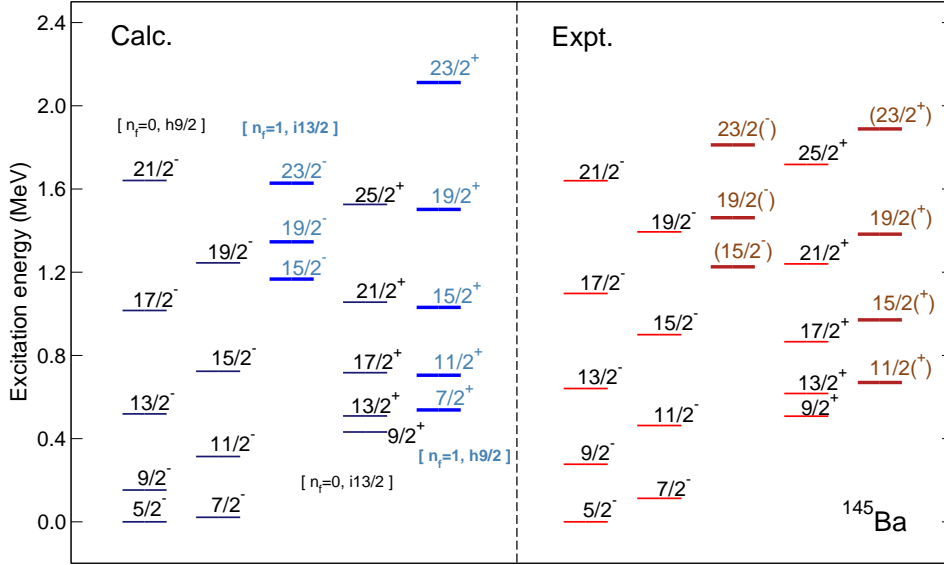


Fig. 9. Calculated and experimental⁶⁵ energy spectra for the low-lying negative- and positive-parity states for the odd- A nucleus ^{145}Ba . Those bands that are suggested to be of octupole nature are highlighted in thick lines. The calculations are performed within the sdf -IBFM that is based on the universal energy functional DD-PC1.

bandhead $9/2_1^+$ is mostly made of the odd neutron in the $1i_{13/2}$ unique-parity orbit coupled to the sd boson space. Experimentally⁶⁵ the observed $\Delta I = 2$ negative-parity band built on the $15/2^-$ state at 1226 keV, and positive-parity band built on the $11/2^+$ state at 670 keV are interpreted as octupole bands. Corresponding theoretical bands are the ones based on the $15/2_4^-$ and $7/2_1^+$ states. These are, respectively, determined by the configurations of the odd neutron in the $1i_{13/2}$ and $1h_{9/2}$ orbits coupled to the boson space containing one f boson ($\langle n_f \rangle \approx 1$). The predicted octupole bands have rather large $E3$ transitions to non-octupole ($\langle n_f \rangle \approx 0$) states: $B(E3; 15/2_4^- \rightarrow 9/2_1^+) = 25$, $B(E3; 19/2_2^- \rightarrow 13/2_1^+) = 31$, $B(E3; 11/2_1^+ \rightarrow 5/2_1^-) = 4.7$, and $B(E3; 15/2_1^+ \rightarrow 9/2_1^-) = 15$ (all in W.u.)

5.2. Shape coexistence and low-lying 0^+ states

Shape coexistence is an intriguing feature of nuclear structure, in which different intrinsic structures appear near the ground state of a single nucleus.^{11,12} Manifestation of the shape coexistence is the existence of low-lying 0^+ excited states close in energy to the ground state. The extra low-lying 0^+ states are interpreted as intruder states arising from the cross-shell multiparticle-multihole excitations. With the particle-hole excitations the residual neutron-proton correlations are increased to such a degree as to lower the 0^+ energies.^{66,67} The different intruder 0^+ states and subsequent bands can also be associated with different intrinsic deformations

in the mean-field potential energy surface.^{68,69}

To incorporate the intruder states in the IBM, one can adopt the prescription proposed by Duval and Barrett,⁷⁰ in which the usual IBM Hilbert space is extended to be a direct sum of the shell-model-like 0p-0h normal, and 2p-2h, 4p-4h, ... intruder configuration spaces. Several independent IBM Hamiltonians, corresponding to different configurations, are introduced and are allowed to be mixed. Assuming that the particle and hole states are not distinguished, these Hamiltonians differ in boson number by two. The total IBM Hamiltonian that is to carry out the configuration mixing of the $2kp-2kh$ ($k = 0, 1, 2, \dots$) states is then given by

$$\hat{H} = \hat{P}_0 \hat{H}_0 \hat{P}_0 + \sum_{k=1} \hat{P}_k (\hat{H}_k + \Delta_k) \hat{P}_k + \sum_{k=0} \hat{P}_{k+1} \hat{V}_{k,k+1} \hat{P}_k + (H.c.). \quad (7)$$

\hat{H}_k is the unperturbed Hamiltonian for the $2kp-2kh$ configuration, the operator \hat{P}_k projects states onto the $2kp-2kh$ space, and the constant Δ_k ($k \geq 1$) represents the energy required to promote $2k$ nucleons (or k bosons) from one major shell to another. The interaction $\hat{V}_{k,k+1}$ admixes the $2kp-2kh$ and $2(k+1)p-2(k+1)h$ configurations, hence does not conserve boson number.

Since the configuration mixing IBM framework significantly alleviates the computational burden often accompanying massive computations as in the large-scale shell model, it has been extensively employed as an alternative approach to shape coexistence. A number of phenomenological studies using the configuration-mixing IBM have been carried out, e.g., for the neutron-deficient Hg,⁷¹ neutron-rich Zr,⁷² and even-even Cd.⁷³ On the other hand, since several independent IBM Hamiltonians and mixing terms are considered, this framework naturally involves a large number of adjustable parameters.

The method of deriving the configuration-mixing IBM Hamiltonian from the SCMF calculation has been developed³⁰ for the description of the quadrupole collective states in the Pb region. More recently, this method was extended to include the f boson degrees of freedom so as to deal with the shape coexistence that involves both quadrupole and octupole states.⁷⁴ The following discussion concerns this new development, taking the nucleus ⁷⁶Kr as a representative case. Note that there are a few instances in which the configuration mixing *sdf* (or *spdf*) IBM has been used in a purely phenomenological way for describing structure of even-even Cd isotopes.^{75,76}

To begin with, two sets of SCMF calculations are performed, with constraints on the triaxial quadrupole (β_2, γ) deformations with $\beta_3 = 0$, and on the axially symmetric quadrupole-octupole (β_2, β_3) deformations. The angle variable γ corresponds to the triaxial deformation, and is defined within the range $0^\circ \leq \gamma \leq 60^\circ$. Figure 10 shows the potential energy surfaces within the (β_2, γ) and (β_2, β_3) planes, computed by the RHB method using the functional DD-PC1 and the separable pairing force. In the β_2 - γ energy surface, a spherical global minimum is obtained and, in addition, an weakly oblate deformed and a strongly prolate deformed local minima can be seen at $(\beta_2, \gamma) \approx (0.2, 60^\circ)$ and $(0.45, 0^\circ)$, respectively. The spherical ground

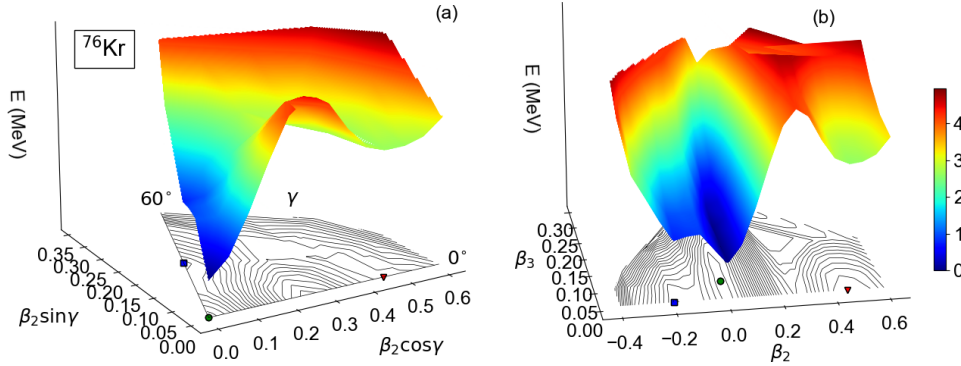


Fig. 10. Potential energy surfaces for ^{76}Kr in terms of the (a) triaxial quadrupole (β_2, γ) and (b) axially-symmetric quadrupole β_2 and octupole β_3 deformations, calculated within the constrained RHB method based on the DD-PC1 functional and separable pairing force. Two dimensional contour plots are also shown, with the energy difference between neighboring contours being 0.2 MeV. The symbols circle, square, and triangle represent the spherical global minimum, and oblate and prolate local minima, respectively.

state reflects the effect of the neutron $N = 40$ subshell closure. The β_2 - β_3 energy surface has the global minimum at $(\beta_2, \beta_3) \approx (0.0, 0.05)$ with non-zero octupole deformation, while the potential is soft along the β_3 deformation.

Since the energy surface exhibits three minima, the IBM space consists of the three configurations corresponding to the 0p-0h, 2p-2h, and 4p-4h states that comprise n , $n + 2$, and $n + 4$ bosons. The normal 0p-0h space here corresponds to the $N/Z = 28$ -50 major shell, hence the boson number $n = 9$. In addition, the unperturbed 0p-0h Hamiltonian is associated with the spherical global minimum on the energy surfaces, while the 2p-2h and 4p-4h Hamiltonians are assigned to the oblate and prolate local minima, respectively. The full configuration mixing *sdf* IBM Hamiltonian is then determined by the procedure described in Ref. 74. The corresponding Hamiltonian is diagonalized in the boson space

$$[(sdf)^n] \oplus [(sdf)^{n+2}] \oplus [(sdf)^{n+4}]. \quad (8)$$

In the middle part of Fig. 11 the low-energy excitation spectra for ^{76}Kr , resulting from the configuration mixing *sdf*-IBM, are compared with the experimental data,^{53,77} and with the usual *sdf*-IBM result obtained by using the single configuration associated with the spherical ground state. In both sets of the *sdf*-IBM, all the negative-parity states are based on the one-*f* boson configuration with the expectation value $\langle \hat{n}_f \rangle \approx 1$, while $\langle \hat{n}_f \rangle \approx 0$ for the positive parity states.

A notable effect of taking into account the configuration mixing is the lowering in energy of the excited 0^+ states. In the usual *sdf*-IBM with the single configuration, the 0_2^+ and 0_3^+ excitation energies are calculated to be $E_x \approx 1.5$ MeV and 3.25 MeV, respectively, whereas they are both $E_x < 1$ MeV in the configuration mixing IBM. The energy levels for the positive-parity yrast states with spin $I > 0$ and also

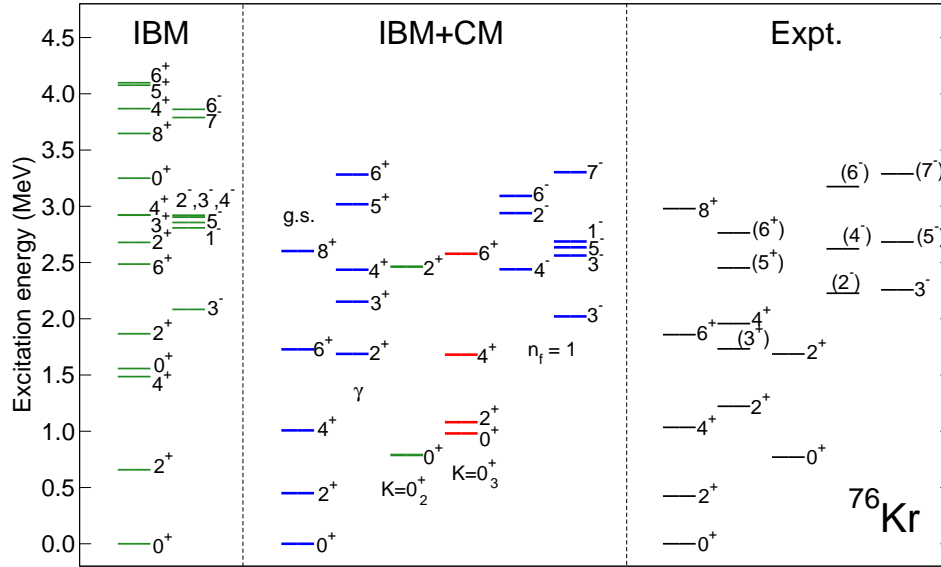


Fig. 11. Excitation spectra for positive- and negative-parity states for ^{76}Kr calculated by using a single configuration (“IBM”) and taking into account the configuration mixing (“IBM+CM”). The IBM calculations are performed with the microscopic basis on the universal functional DD-PC1. Experimental data^{53,77} are shown on the right.

for the negative-parity states are generally lowered as a result of the mixing. A near degeneracy of the 1_1^- , 2_1^- , 3_2^- , 4_1^- , and 5_1^- levels, obtained in the single-configuration calculation, can be interpreted as a quintet arising from the quadrupole-octupole phonon coupling $2^+ \otimes 3^-$. The degeneracy is, however, removed in the configuration mixing calculation as a consequence of the level repulsion.

Regarding the transition properties, the $B(E3; 3_1^- \rightarrow 0_1^+)$ rates are calculated to be ≈ 30 W.u. in this mass region⁷⁴. An effect of the configuration mixing is, for instance, increase of the ratio $B(E3; 3_1^- \rightarrow 2_1^+)/B(E3; 3_1^- \rightarrow 0_1^+)$ by an order of magnitude. However, experimental data for the $E3$ and $E1$ transitions in this region are scarce, and a more thorough assessment of the model remains to be done.

To analyze in more detail the nature of the proposed low-spin bands, Fig. 12 shows compositions of the spherical (0p-0h), oblate (2p-2h), and prolate (4p-4h) configurations in the wave functions of the members of these bands. Even though the spherical ground state is predicted at the SCMF level, at the IBM level the oblate 2p-2h configuration constitutes most of the wave functions for the ground-state and γ bands, and all the negative-parity states shown in Fig. 11. The $K^\pi = 0_2^+$ band with the bandhead 0_2^+ state is, in turn, spherical in nature. However, substantial amounts of the oblate and prolate components are admixed into the members of the proposed $K^\pi = 0_2^+$ band. The $K^\pi = 0_3^+$ rotational-like band based upon the 0_3^+ state is dominated by the strongly deformed prolate configuration.

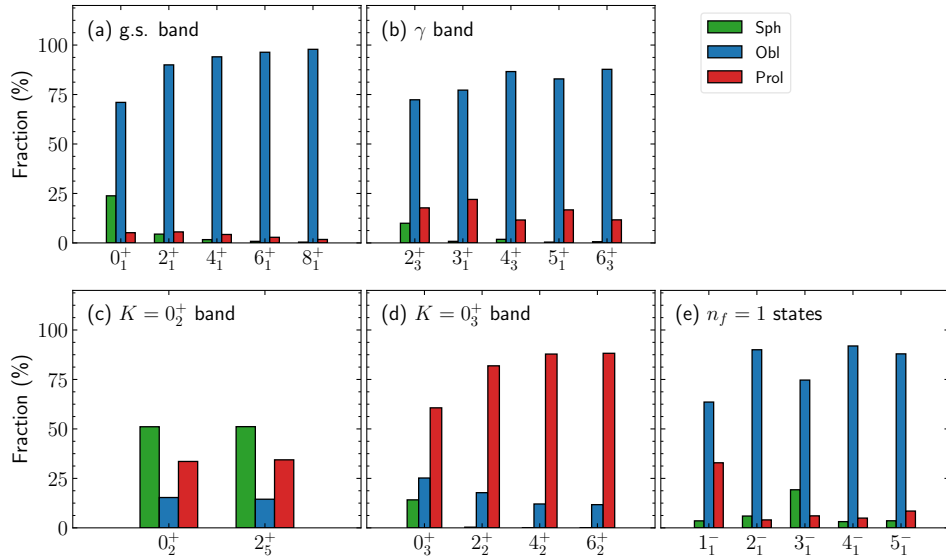


Fig. 12. Compositions of the spherical, oblate, and prolate configurations in the wave functions of the positive-parity states belonging to the (a) ground-state, (b) γ -, (c) $K^\pi = 0_2^+$, and (d) $K^\pi = 0_3^+$ bands, and of the (e) low-spin negative-parity (one f boson, $n_f = 1$) states for ^{76}Kr .

5.3. Double octupole phonon states

A number of low-lying excited 0^+ states are also observed in those nuclei in rare-earth region.⁷⁸ Microscopic origin of these 0^+ states is under active debate, and has been attributed, e.g., to the pairing vibrations,^{79,80} intruder excitations,⁸¹ and coupling of the double octupole phonons.⁸² To explain the occurrence of these low-energy 0^+ states the *sdf*- or *spdf*-IBM has often been used. In particular, calculation within the *sdf*-IBM that is based on the Gogny EDF has shown³³ that the 0_2^+ excited states in many of the Sm and Gd nuclei are formed mainly by the coupling of two f bosons. The double octupole phonon nature of the 0_2^+ state has been suggested in light actinides as well within the *sdf*-IBM calculation based on the relativistic EDF.³²

5.4. Coupling with p boson

A straightforward extension of the *sdf*-boson model would be to include the dipole p boson. Inclusion of this boson degree of freedom would indeed improve the description of the negative-parity levels and their $E1$ transition properties,⁸³ and has also been considered in the calculations on the α -clustering phenomena.^{84–87} At the microscopic level, it was shown,⁸⁸ by using the Nilsson model, that large amount of the dipole pair, i.e., p boson, component is contained in the wave functions of negative-parity states, and that the dipole boson is as essential a degree of freedom

as the octupole one. The physical meaning of the p boson has been attributed to the center of mass motion or giant dipole resonance,^{88,89} but is not as entirely clear as that of the f boson, since the dipole mode is more or less of single-particle nature.

6. Conclusions

We have reviewed recent theoretical investigations of the octupole shapes and collective excitations in nuclei within the *sdf*-IBM that is formulated microscopically using the nuclear EDF framework. The illustrative application to Th isotopes has shown the occurrence of the stable octupole state around $N = 134$ as well as the shape phase transition that involves both quadrupole and octupole modes. A global spectroscopic study has confirmed the enhancement of the octupole collectivity in a wide mass region. The coupling between the octupole and additional degrees of freedom has been shown to play a role in the descriptions of a variety of related nuclear structure phenomena, including the shape coexistence.

The present model descriptions are based on the assumptions that the nuclear EDFs, upon which the IBM Hamiltonian is built, provide for all nuclei the correct mean-field properties (potential energy surfaces, single-particle energies, etc.), and that the EDF-to-IBM mapping procedure is valid. In this respect, for a more refined description of the octupole-related properties, further improvements of the method would be made, e.g., through (i) the assessment of the capability of a given EDF of predicting complex nuclear shape phenomena as well as spectroscopy, (ii) the inclusions of additional terms in the boson Hamiltonian and/or degrees of freedom, such as the p boson, in the boson space, and (iii) the microscopic derivation of the boson effective charges for the $E1$ and $E3$ transition operators.

Furthermore, the theoretical method discussed throughout this paper has a potential to explore problems in interdisciplinary fields. For instance, the semi-microscopic *sdf*-IBFM, described in Sec. 5.1, can be used to study the proposed parity doublet and EDM for the odd-mass Ra and Th isotopes, which serve as a testing ground for the CP symmetry violation.⁹⁰

Acknowledgements

The author thanks D. Vretenar, T. Nikšić, L. M. Robledo, and R. Rodríguez-Guzmán for their contributions to the works discussed in this paper. The author has been supported by the Tenure Track Pilot Programme of the Croatian Science Foundation and the École Polytechnique Fédérale de Lausanne, and the Project TTP-2018-07-3554 Exotic Nuclear Structure and Dynamics, with funds of the Croatian-Swiss Research Programme.

References

1. P. A. Butler and W. Nazarewicz, *Rev. Mod. Phys.* **68** (1996) 349.
2. P. A. Butler, *J. Phys. G: Nucl. Part. Phys.* **43** (2016) 073002.

3. L. P. Gaffney *et al.*, *Nature (London)* **497** (2013) 199.
4. M. M. R. Chishti *et al.*, *Nat. Phys.* **16** (2020) 853.
5. P. A. Butler *et al.*, *Phys. Rev. Lett.* **124** (2020) 042503.
6. B. Bucher *et al.*, *Phys. Rev. Lett.* **116** (2016) 112503.
7. B. Bucher *et al.*, *Phys. Rev. Lett.* **118** (2017) 152504.
8. J. Engel, M. J. Ramsey-Musolf and U. van Kolck, *Prog. Part. Nucl. Phys.* **71** (2013) 21 .
9. F. Iachello and A. Arima, *The interacting boson model* (Cambridge Univ. Press, Cambridge, UK, 1987).
10. P. Cejnar, J. Jolie and R. F. Casten, *Rev. Mod. Phys.* **82** (2010) 2155.
11. J. L. Wood, K. Heyde, W. Nazarewicz, M. Huyse and P. van Duppen, *Phys. Rep.* **215** (1992) 101 .
12. K. Heyde and J. L. Wood, *Rev. Mod. Phys.* **83** (2011) 1467.
13. A. Arima and F. Iachello, *Phys. Rev. Lett.* **35** (1975) 1069.
14. T. Otsuka, A. Arima, F. Iachello and I. Talmi, *Phys. Lett. B* **76** (1978) 139 .
15. T. Otsuka, A. Arima and F. Iachello, *Nucl. Phys. A* **309** (1978) 1.
16. A. Arima and F. Iachello, *Ann. Phys. (NY)* **111** (1978) 201 .
17. J. Engel and F. Iachello, *Phys. Rev. Lett.* **54** (1985) 1126.
18. J. Engel and F. Iachello, *Nucl. Phys. A* **472** (1987) 61 .
19. A. F. Barfield *et al.*, *Ann. Phys.* **182** (1988) 344 .
20. N. V. Zamfir and D. Kusnezov, *Phys. Rev. C* **63** (2001) 054306.
21. P. D. Cottle and N. V. Zamfir, *Phys. Rev. C* **54** (1996) 176.
22. D. Kusnezov and F. Iachello, *Phys. Lett. B* **209** (1988) 420 .
23. D. Kusnezov, *J. Phys. A: Math. Gen.* **22** (1989) 4271.
24. D. Kusnezov, *J. Phys. A: Math. Gen.* **23** (1990) 5673.
25. T. Mizusaki and T. Otsuka, *Prog. Theor. Phys. Suppl.* **125** (1996) 97.
26. K. Nomura, N. Shimizu and T. Otsuka, *Phys. Rev. Lett.* **101** (2008) 142501.
27. K. Nomura, N. Shimizu and T. Otsuka, *Phys. Rev. C* **81** (2010) 044307.
28. K. Nomura, T. Otsuka, N. Shimizu and L. Guo, *Phys. Rev. C* **83** (2011) 041302.
29. K. Nomura, N. Shimizu, D. Vretenar, T. Nikšić and T. Otsuka, *Phys. Rev. Lett.* **108** (2012) 132501.
30. K. Nomura, R. Rodríguez-Guzmán, L. M. Robledo and N. Shimizu, *Phys. Rev. C* **86** (2012) 034322.
31. K. Nomura, D. Vretenar and B.-N. Lu, *Phys. Rev. C* **88** (2013) 021303.
32. K. Nomura, D. Vretenar, T. Nikšić and B.-N. Lu, *Phys. Rev. C* **89** (2014) 024312.
33. K. Nomura, R. Rodríguez-Guzmán and L. M. Robledo, *Phys. Rev. C* **92** (2015) 014312.
34. K. Nomura, T. Nikšić and D. Vretenar, *Phys. Rev. C* **93** (2016) 054305.
35. K. Nomura, R. Rodríguez-Guzmán and L. M. Robledo, *Phys. Rev. C* **101** (2020) 044318.
36. K. Nomura, R. Rodríguez-Guzmán and L. M. Robledo, *Phys. Rev. C* **101** (2020) 024311.
37. M. Bender, P.-H. Heenen and P.-G. Reinhard, *Rev. Mod. Phys.* **75** (2003) 121.
38. D. Vretenar, A. V. Afanasjev, G. A. Lalazissis and P. Ring, *Phys. Rep.* **409** (2005) 101 .
39. T. Nikšić, D. Vretenar and P. Ring, *Prog. Part. Nucl. Phys.* **66** (2011) 519.
40. L. M. Robledo, T. R. Rodríguez and R. R. Rodríguez-Guzmán, *J. Phys. G: Nucl. Part. Phys.* **46** (2019) 013001.
41. N. Schunck (ed.), *Energy Density Functional Methods for Atomic Nuclei* (IOP Publishing, 2019).

42. P. Ring and P. Schuck, *The Nuclear Many-Body Problem* (Springer, Berlin, 1980).
43. T. Nikšić, D. Vretenar and P. Ring, *Phys. Rev. C* **78** (2008) 034318.
44. Y. Tian, Z. Y. Ma and P. Ring, *Phys. Lett. B* **676** (2009) 44 .
45. Z. P. Li, T. Nikšić and D. Vretenar, *J. Phys. G: Nucl. Part. Phys.* **43** (2016) 024005.
46. J. N. Ginocchio and M. W. Kirson, *Nucl. Phys. A* **350** (1980) 31.
47. A. E. L. Dieperink, O. Scholten and F. Iachello, *Phys. Rev. Lett.* **44** (1980) 1747.
48. A. Bohr and B. R. Mottelson, *Phys. Scr.* **22** (1980) 468.
49. K. Nomura, L. Lotina, T. Nikšić and D. Vretenar, *Phys. Rev. C* **103** (2021) 054301.
50. K. Nomura *et al.*, *Phys. Rev. C* **102** (2020) 064326.
51. Z. P. Li *et al.*, *Phys. Lett. B* **726** (2013) 866 .
52. S. Y. Xia *et al.*, *Phys. Rev. C* **96** (2017) 054303.
53. Brookhaven National Nuclear Data Center. <http://www.nndc.bnl.gov>.
54. K. Nomura *et al.*, *Phys. Rev. C* **103** (2021) 044311.
55. K. Nomura *et al.*, *Phys. Rev. C* **104** (2021) 044324.
56. K. Nomura *et al.*, *Phys. Rev. C* **104** (2021) 054320.
57. S. Goriely, S. Hilaire, M. Girod and S. Péru, *Phys. Rev. Lett.* **102** (2009) 242501.
58. J. Decharge and M. Girod and D. Gogny, *Phys. Lett. B* **55** (1975) 361.
59. T. Kibédi and R. H. Spear, *At. Data and Nucl. Data Tables* **80** (2002) 35 .
60. G. de Angelis *et al.*, *Phys. Lett. B* **535** (2002) 93.
61. F. Iachello and P. Van Isacker, *The interacting boson-fermion model* (Cambridge Univ. Press, Cambridge, UK, 1991).
62. F. Iachello and O. Scholten, *Phys. Rev. Lett.* **43** (1979) 679.
63. K. Nomura, T. Nikšić and D. Vretenar, *Phys. Rev. C* **97** (2018) 024317.
64. O. Scholten, *Prog. Part. Nucl. Phys.* **14** (1985) 189.
65. T. Rzaca-Urban *et al.*, *Phys. Rev. C* **86** (2012) 044324.
66. P. Federman and S. Pittel, *Phys. Lett. B* **69** (1977) 385 .
67. K. Heyde *et al.*, *Nucl. Phys. A* **466** (1987) 189 .
68. R. Bengtsson *et al.*, *Phys. Lett. B* **183** (1987) 1.
69. W. Nazarewicz, *Phys. Lett. B* **305** (1993) 195 .
70. P. D. Duval and B. R. Barrett, *Phys. Lett. B* **100** (1981) 223.
71. J. E. García-Ramos and K. Heyde, *Phys. Rev. C* **89** (2014) 014306.
72. N. Gavrielov, A. Leviatan and F. Iachello, *Phys. Rev. C* **99** (2019) 064324.
73. A. Leviatan *et al.*, *Phys. Rev. C* **98** (2018) 031302.
74. K. Nomura, *Phys. Rev. C* **106** (2022) 024330.
75. P. E. Garrett *et al.*, *Phys. Rev. C* **59** (1999) 2455.
76. D. Bandyopadhyay *et al.*, *Phys. Rev. C* **68** (2003) 014324.
77. E. Clément *et al.*, *Phys. Rev. C* **75** (2007) 054313.
78. A. Aprahamian *et al.*, *Phys. Rev. C* **98** (2018) 034303.
79. J. Xiang *et al.*, *Phys. Rev. C* **101** (2020) 064301.
80. K. Nomura, D. Vretenar, Z. P. Li and J. Xiang, *Phys. Rev. C* **102** (2020) 054313.
81. P. Van Isacker *et al.*, *Nucl. Phys. A* **380** (1982) 383 .
82. N. V. Zamfir, J.-y. Zhang and R. F. Casten, *Phys. Rev. C* **66** (2002) 057303.
83. M. Sugita, T. Otsuka and P. von Brentano, *Phys. Lett. B* **389** (1996) 642 .
84. F. Iachello and A. Jackson, *Phys. Lett. B* **108** (1982) 151.
85. H. Daley and F. Iachello, *Phys. Lett. B* **131** (1983) 281.
86. M. Spieker, S. Pascu, A. Zilges and F. Iachello, *Phys. Rev. Lett.* **114** (2015) 192504.
87. R. Bijker and F. Iachello, *Nucl. Phys. A* **957** (2017) 154.
88. T. Otsuka, *Phys. Lett. B* **182** (1986) 256 .
89. T. Otsuka and M. Sugita, *Phys. Lett. B* **209** (1988) 140 .
90. J. Dobaczewski and J. Engel, *Phys. Rev. Lett.* **94** (2005) 232502.